Supporting Information

Silver-incorporated NiCo metal-organic frameworks with controlled morphology for enhanced cycling in flexible supercapacitors application

Chu Chu[a], Wenjing Zhang[a,c], Xuehua Yan[a,b,*], Yingnan Yan[a], Jianmei Pan[a], Zohreh Shahnavaz[b], Jamile Mohammadi Moradian[b]

[a]*School of Materials Science and Engineering, Jiangsu University, Zhenjiang 212013, China*

[b]*Institute for Advanced Materials, Jiangsu University, Zhenjiang 212013, China*

[c]*School of Materials Science and Engineering, Tongji University, Shanghai 200082, China*

*Corresponding author: Xuehua Yan; E-mail address: xhyan@ujs.edu.cn (X.H Yan)

Analytical techniques

X-ray diffraction (XRD, D8 ADVANCE) analysis was employed to determine the crystal structures of the prepared materials with a scanning range of 5°-90° and 5°-30° angels. A Raman spectrometer (DXR) was used to qualitatively analyze the prepared materials. The elemental compositions and atomic valence states of the composites were investigated using X-ray photoelectron spectroscopy (XPS, Thermo ESCALAB 250Xi). The morphology of the product was examined by field-emission scanning electron microscopy (SEM, JEOL JSM-7800F). N_2 adsorption-desorption isotherms were measured using a Micromeritics 3Flex instrument, and the sample was degassed for 6 h at 120 °C. ICP-OES data were obtained using Thermo Fisher iCAP PRO. The HRTEM analysis was conducted using a Thermo Fisher TF-20 instrument, which allowed for the evaluation of element distribution and interplanar spacing within the materials. The Brunauer-Emmett-Teller (BET) surface area analysis, along with nitrogen (N_2) adsorption and desorption isotherms recorded at 77 K, was performed utilizing the NOVA 3000e surface area and pore size analyzer from Quantachrome Instruments, Florida. Before analysis, the samples were degassed under vacuum conditions at 150 °C for a duration of 3 h. To determine the pore size distribution and total pore volume of the samples, the Barrett-Joyner-Halenda (BJH) method was employed.

Electrochemical measurements

According to the GCD diagram, the specific capacitance can be calculated using the

equation S1 and is expressed as follows:

$$C_S = \frac{I\Delta t}{m\Delta V} \quad \text{(S1)}$$

where I is the discharge current, Δt is the discharge time, m is the mass of the prepared electrode, *and* ΔV is the voltage window of the test system.

Moreover, the coulombic efficiency η of the capacitor cell can be calculated from the GCD experiments using equation S2, which is expressed as

$$\eta = \frac{\Delta t_D}{\Delta t_C} \quad \text{(S2)}$$

where Δt_D and Δt_C are the number of discharge and charge cycles, respectively.

The total voltammetric charge (q_T*), along with the outer voltammetric charge (q_O*) and inner voltammetric charge (q_I*), were determined using equations (S4), (S5) and (S6) [1]。

$$(q*)^{-1} = (q_T*)^{-1} + kv^{1/2} \quad \text{(S3)}$$

$$q* = q_O* + k'v^{-1/2} \quad \text{(S4)}$$

$$q_T* = q_O* + q_T* \quad \text{(S5)}$$

The surface capacitance and diffusion contributions to the total charge storage can be calculated using the following equation:

$$i(V) = k_1 v + k_2 v^{1/2} \quad \text{(S6)}$$

where i(V) signifies the current output at potential V, v denotes the scan rate, and k_1v and $k_2v^{1/2}$ are constants that correspond to capacitor control resulting from surface charge adsorption and diffusion control stemming from the redox reaction, respectively.

Electrochemical analysis of the flexible quasi-solid state symmetric SCs

The energy density (Wh/kg) and power density (W/kg) could be calculated by equation(s) S7 and S8:

$$E = \frac{C\Delta V^2}{7.2} \quad \text{(S7)}$$

$$P = \frac{E \times 3600}{\Delta t} \quad \text{(S8)}$$

where C, ΔV, and Δt are the specific capacitance (F/g), working potential (V), and discharge period (s), respectively, of the device.

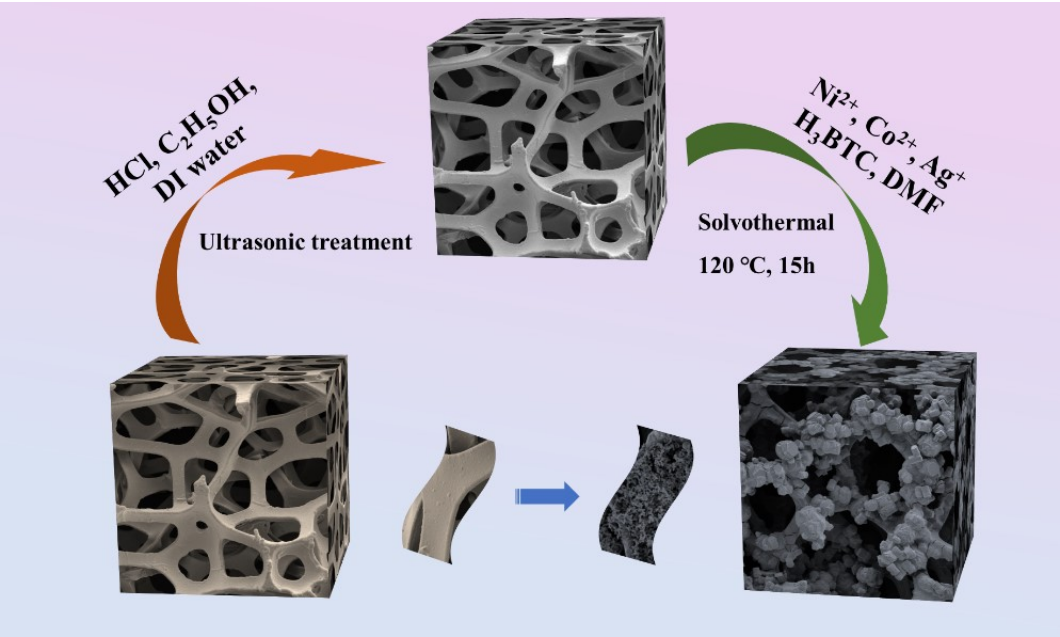

Figure S1 Schematic representation of Ag-incorporated flexible NiCo-MOF/NF electrode materials synthesis.

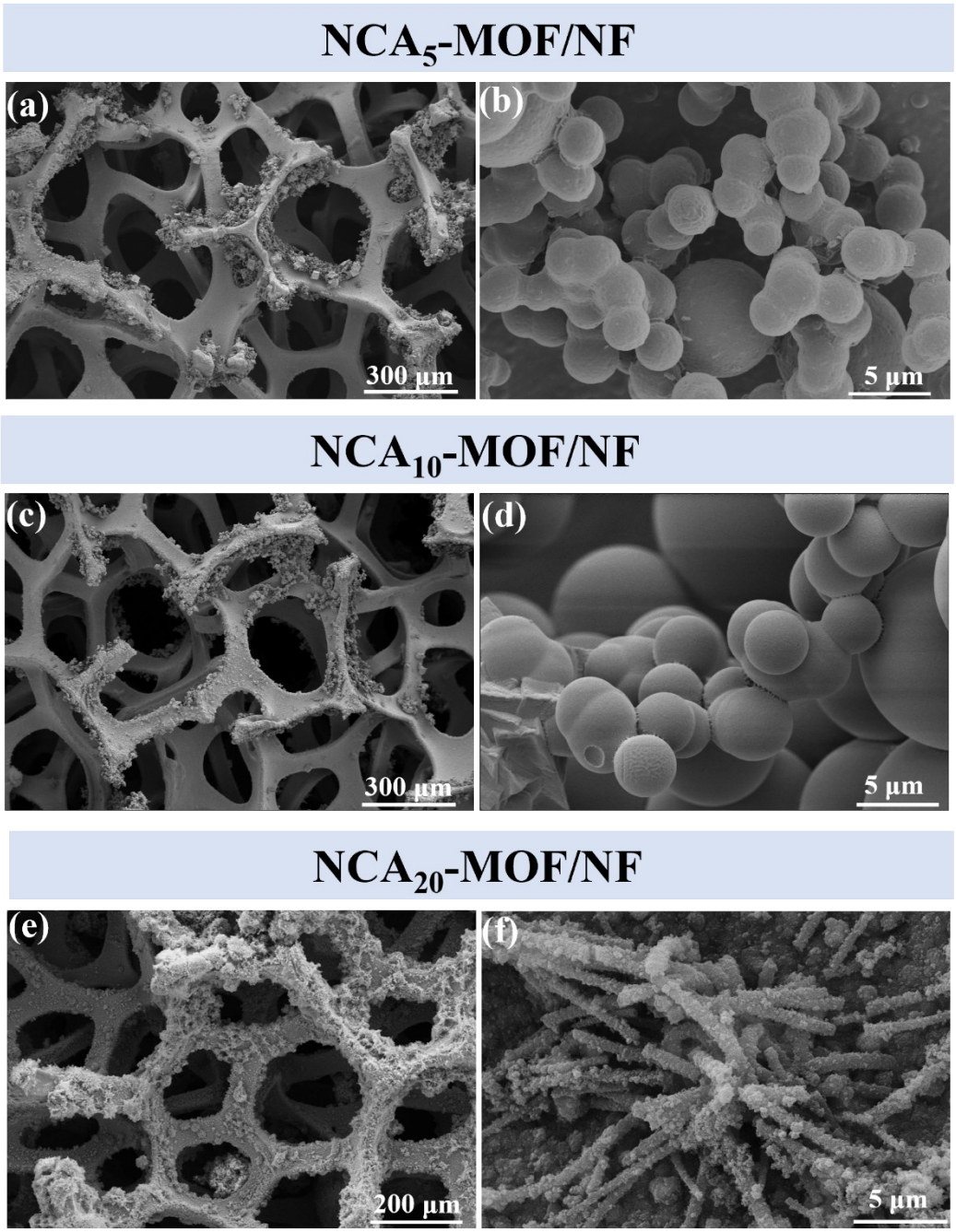

92

93 **Figure S2** SEM images of **(a, b)** NCA_5-MOF/NF, **(c, d)** NCA_{10}-MOF/NF, and **(e, f)** NCA_{20}-

94 MOF/NF electrodes.

95

96

97

98

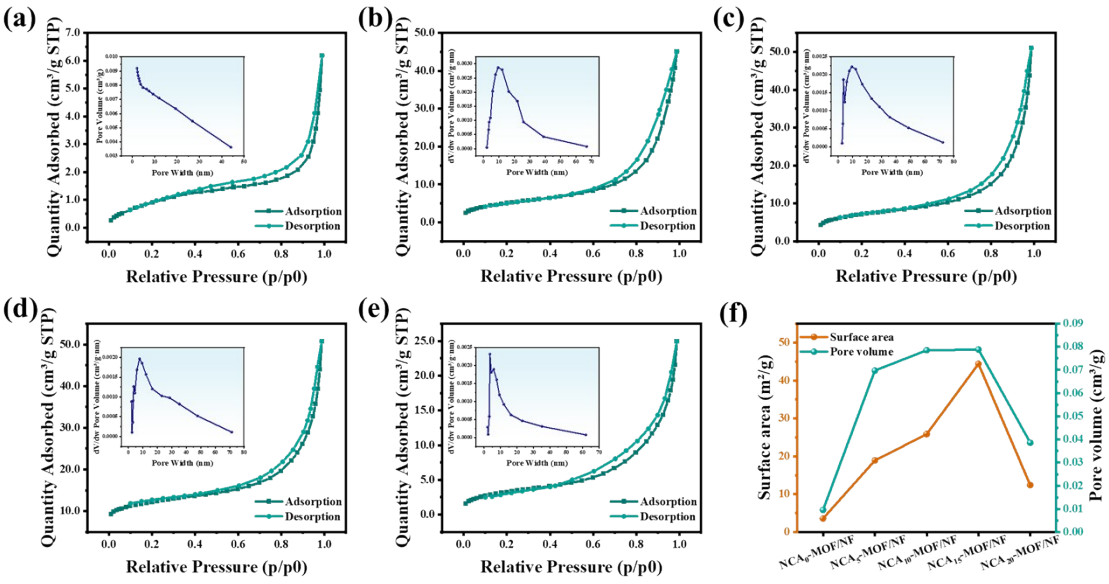

Figure S3 (a-e) N_2 adsorption-desorption isotherm with corresponding pore size distribution, and **(f)** Specific surface area and pore volume of NCA_X-MOF/NF electrodes.

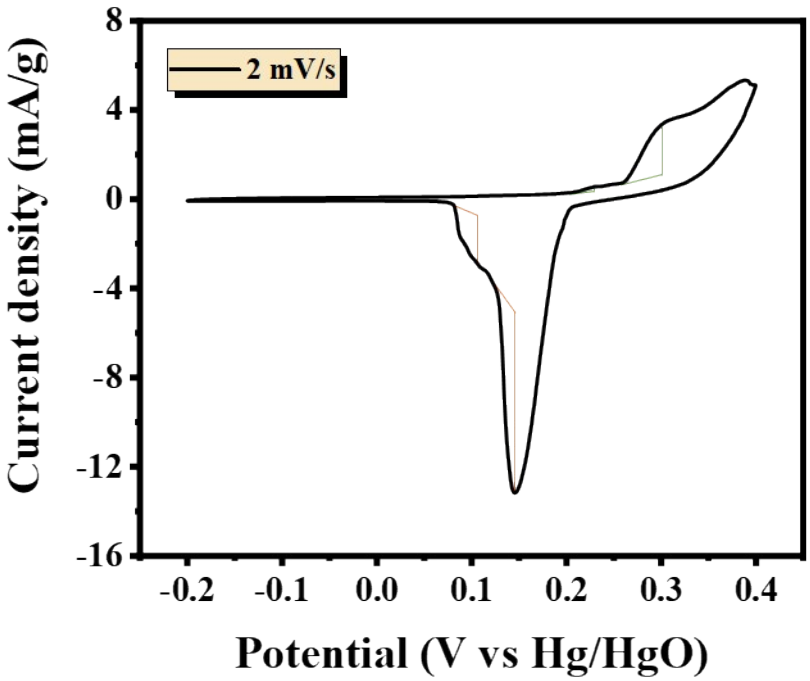

Figure S4 CV curve of NCA_{15}-MOF/NF at a scan rate of 2 mV/s, displaying low reversibility with a broadened anodic peak.

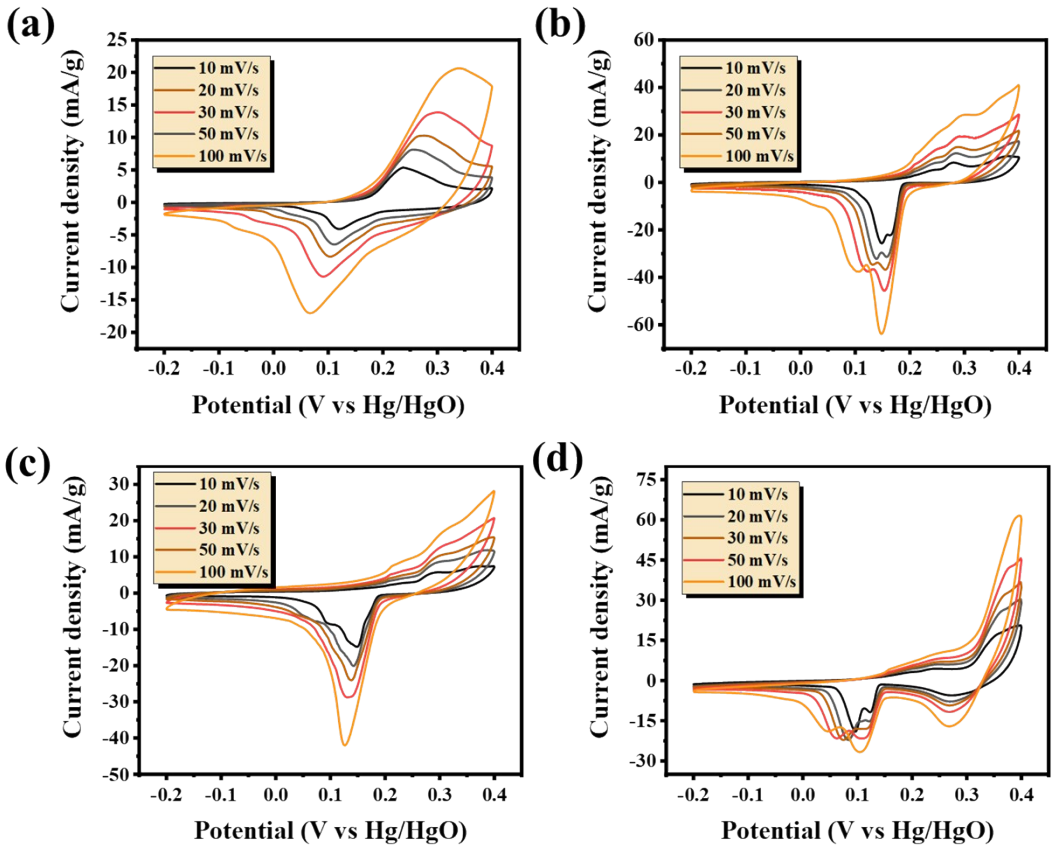

Figure S5 The CVs of **(a)** NCA_0-MOF/NF, **(b)** NCA_5-MOF/NF, **(c)** NCA_{10}-MOF/NF, **(d)** NCA_{20}-MOF/NF electrodes at different scan rates (from 10 mV/s to 100 mV/s) between -0.2 V to 0.4 V (vs. Hg/HgO).

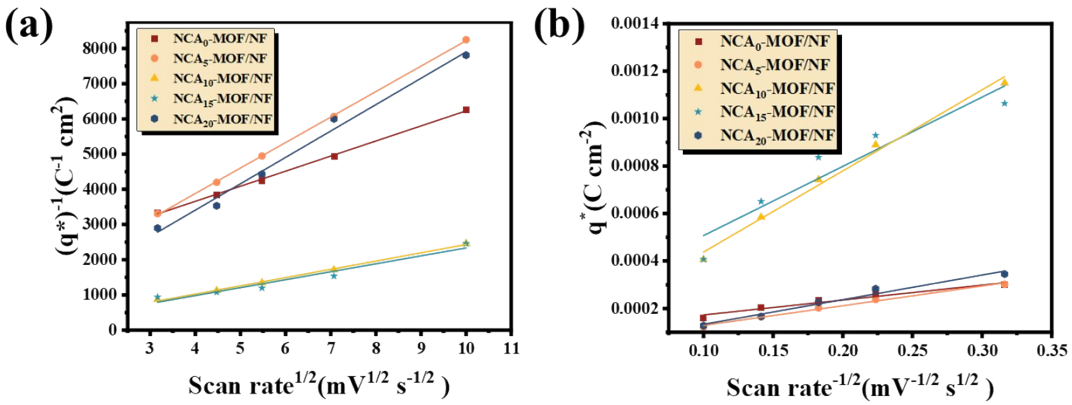

Figure S6 Relationship between **(a)** Reciprocal voltammetric charge $(q*)^{-1}$ and the square root of the scan rate $(v^{1/2})$, and **(b)** Voltammetric charge $(q*)$ and the reciprocal square root of the scan rate $(v^{-1/2})$.

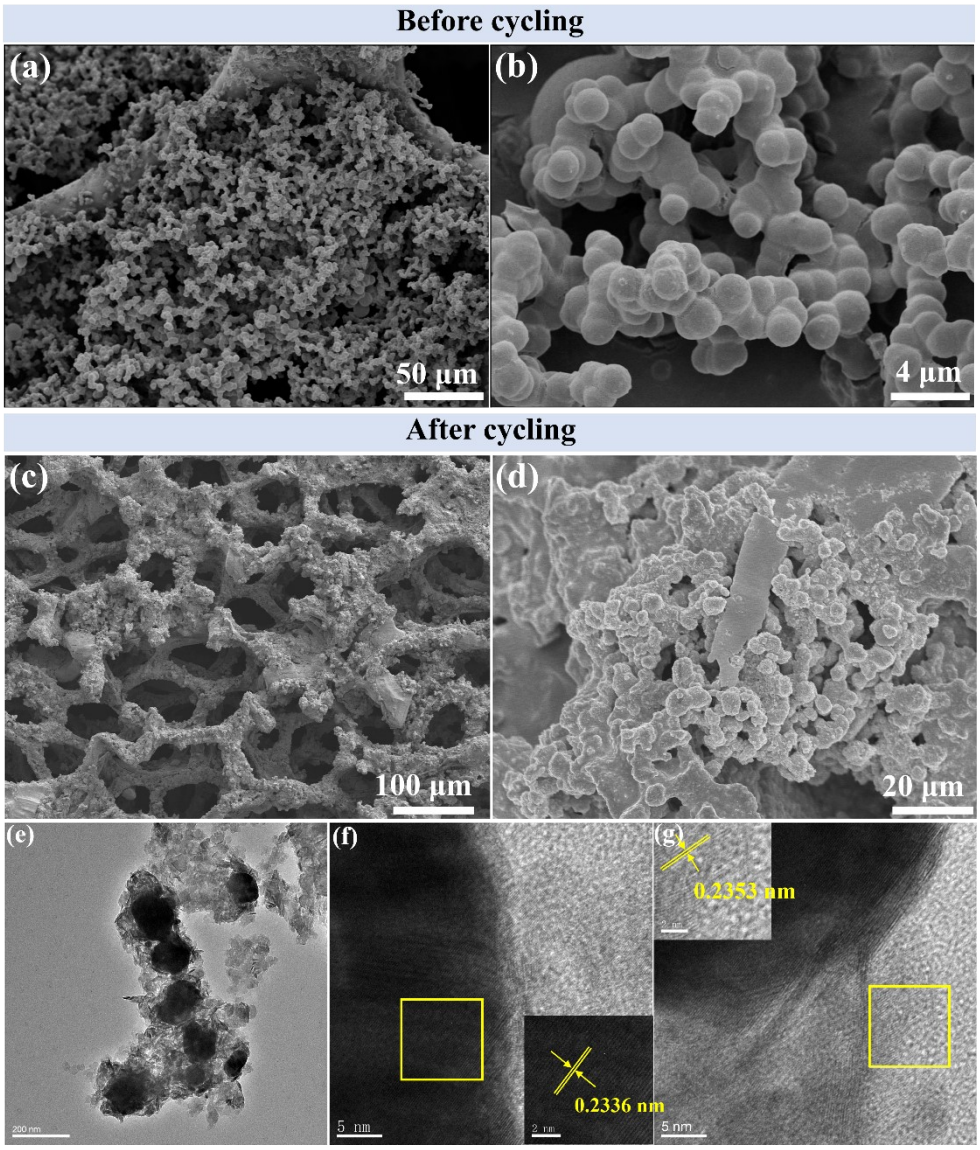

Figure S7 SEM images of NCA_{15}-MOF/NF: **(a, b)** before and (c, d) after cycling tests. NCA_{15}-MOF after cycling: **(e)** HRTEM image, **(f)** lattice spacing of Ag particles in NiCo-LDH, and **(g)** lattice spacing of NiCo-LDH structure formed around Ag particles.

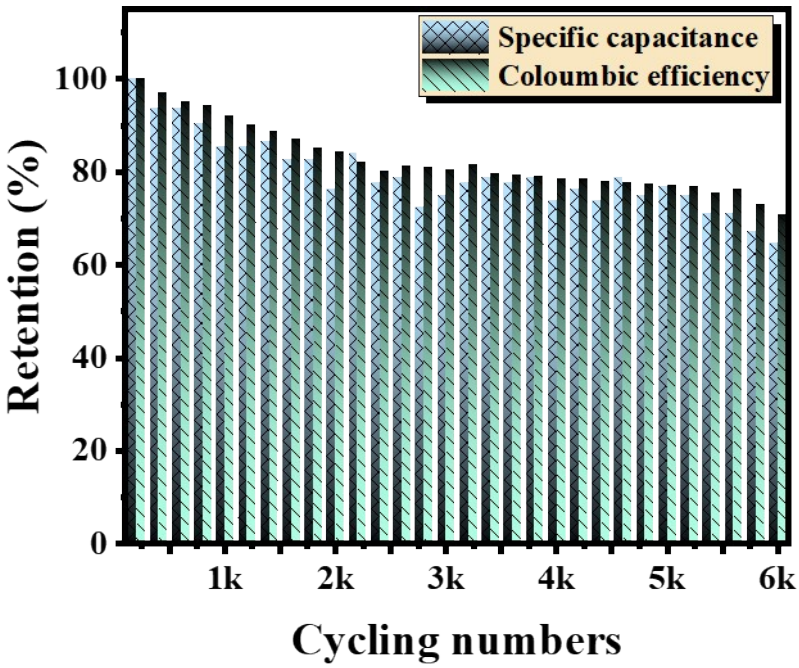

Figure S8. Cycling stability of the NCA_0-MOF/NF electrode material at a current density of 5 A/g over 6,000 cycles. The specific capacitance retention and Coulombic efficiency decreased to 64.68% and 70.8%, respectively.

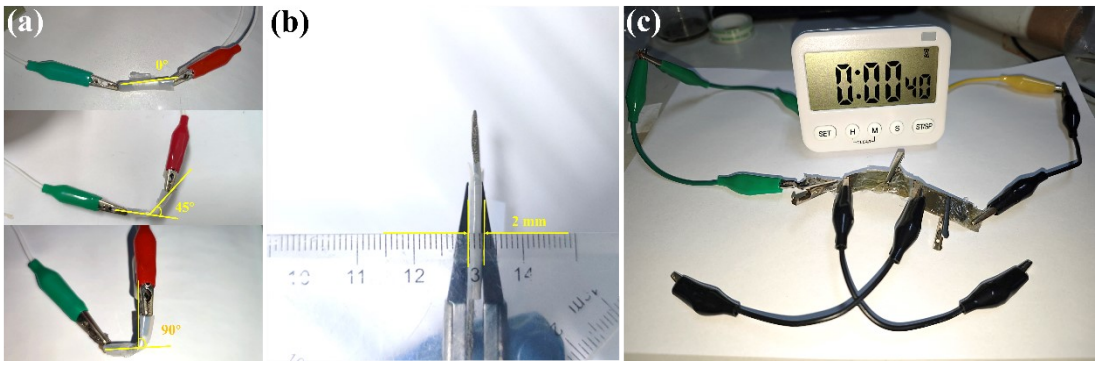

Figure S9. Photograph of the flexible SCs device: **(a)** Flexibility tests at angels 0°, 45°, and 90°, **(b)** The thickness schematic of approximately 2 mm, and **(c)** A fully charged device can test the timer to work properly.

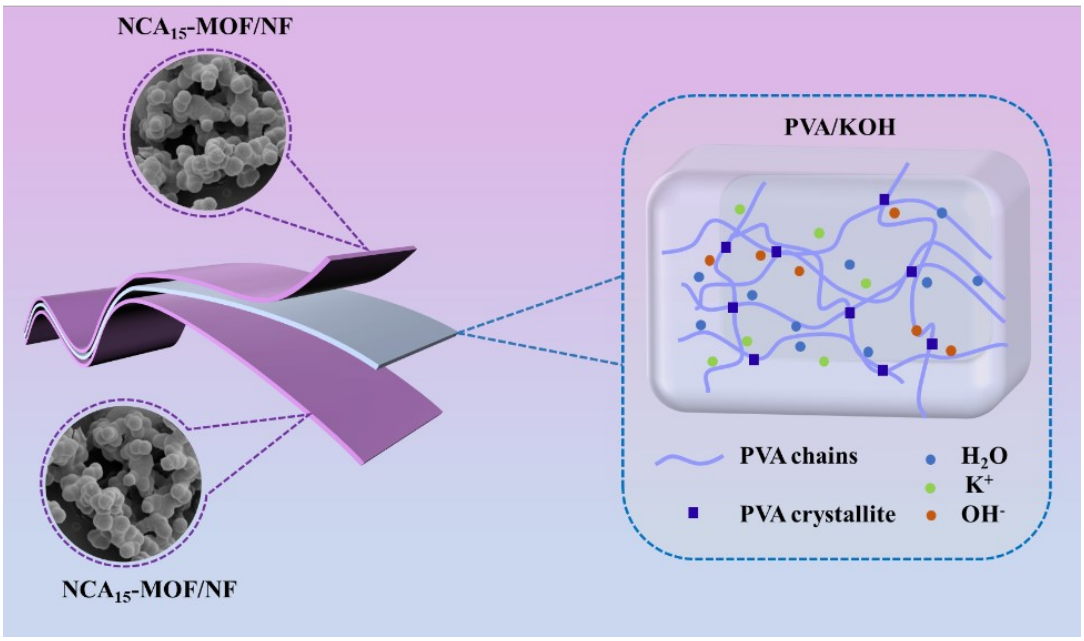

Figure S10 Schematic representation of flexible quasi-solid symmetrical SCs.

Table S1. Ag concentration in various NCA_X-MOF/NF samples analyzed by ICP-MS.

Materials	Ag concentration (mg/g)
NCA_5-MOF/NF	15.92
NCA_{10}-MOF/NF	26.26
NCA_{15}-MOF/NF	38.90
NCA_{20}-MOF/NF	64.36

Table S2 Voltammetric charges and electrochemical porosity of the electrodes.

Materials	q_T (mC cm^{-2})	q_O (mC cm^{-2})	q_I (mC cm^{-2})	q_I /q_T
NCA_0-MOF/NF	0.514	0.100	0.414	80.53%
NCA_5-MOF/NF	1.014	0.456	0.557	54.97%
NCA_{10}-MOF/NF	11.411	0.959	10.451	91.59%
NCA_{15}-MOF/NF	12.710	0.215	12.494	98.31%
NCA_{20}-MOF/NF	2.414	0.030	2.384	98.77%

Table S3 Comparison of energy storage performance of MOF-based electrode materials in symmetrical SCs devices with previously reported materials.

Materials	Synthesis approach	Specific capacitance	Device electrolyte	Device performance after cycling	Refs.
Zn-BTC MOF	Annealing	285 F/g at 1 A/g	6.0 M KOH and 1.0 M Na_2SO_4	89.4% after 10,000 80% after 10,000	[2]
NGCA(ZIF-8)	Sol-gel process	125 F/g at 0.5 A/g	1.0 M Na_2SO_4	93% after 5,000	[3]
Zn–In–S/C@CuO	Solvothermal	245 C/g at 2 A/g	3.0 M KOH	117% after 20,000	[4]
Cu-MOF/rGO	Filtration and ultrasonication	867.09 F/g at 1 A/g	1.0 M PVA/$NaNO_3$	90.07% after 10,000	[5]
Zn-MOF-rGO	Hydrothermal	82.5 F/g at 1 A/g	3.0 M KOH	87% after 5,000	[6]
Zn-BTC@$Ag_5[BW_{12}O_{40}]$	Precipitation	161.7 F/g at 1 A/g	1.0 M Na_2SO_4	91.4% after 5,000	[7]
HHMCN(Zn-MOF-74)	Solvothermal and sulfurization	287 F/g at 0.5 A/g	2.0 M H_2SO_4	95.3% over 10,000	[8]
NCA_{15}-MOF/NF	Hydrothermal	1317 F/g at 1 A/g	3.0 M PVC/KOH	85.9% after 8,000	This study

References

[1] Pahlevani L, Mozdianfard M R, Fallah N. Electrochemical oxidation treatment of offshore produced water using modified Ti/Sb-SnO2 anode by graphene oxide. Journal of Water Process Engineering, 2020, 35: 101204.

[2] Liu N, Liu X, Pan J. A new rapid synthesis of hexagonal prism Zn-MOF as a precursor at room temperature for energy storage through pre-ionization strategy. J Colloid Interface Sci, 2022, 606: 1364-1373.

[3] Ping Y, Yang S, Han J, et al. N-self-doped graphitic carbon aerogels derived from metal–organic frameworks as supercapacitor electrode materials with high-performance. Electrochimica Acta, 2021, 380: 138237.

[4] Hussain I, Ansari M Z, Lamiel C, et al. In Situ Grown Heterostructure Based on MOF-Derived Carbon Containing n-Type Zn–In–S and Dry-Oxidative p-Type CuO as Pseudocapacitive Electrode Materials. ACS Energy Letters, 2023, 8(4): 1887-1895.

[5] Sarathkumar Krishnan A K G, Mayank K. Singh, Nikita Guha, Dhirendra K. Rai. Nitrogen-rich Cu-MOF decorated on reduced graphene oxide nanosheets for hybrid supercapacitor applications with enhanced cycling stability. Chemical Engineering Journal, 2022, 435:135042.

[6] Thi Q V, Patil S A, Katkar P K, et al. Electrochemical performance of zinc-based metal-organic framework with reduced graphene oxide nanocomposite electrodes for supercapacitors. Synthetic Metals, 2022, 290: 117155.

[7] Wang L, Kang N, Gong L, et al. A novel core-shell structured hybrid composed of zinc homobenzotrizoate and silver borotungstate with supercapacitor and photocatalytic dye degradation performance. Journal of Energy Storage, 2022, 46: 103873.

[8] Li M, Zhang W, Liu T, et al. Hierarchical hollow microspheres of carbon nanorods with enhanced supercapacitor performance. Materials Today Communications, 2021, 28: 102500.